EUROPEAN ORGANIZATION FOR NUCLEAR RESEARCH
European Laboratory for Particle Physics

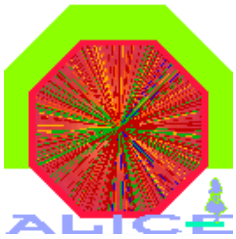

Internal Note/TPC
ALICE reference number
ALICE-INT-2005-029 version 1.0
Institute reference number
[-]
Date of last change
26.10.2005

Performance Test of the ALICE TPC IROC Module at the PS

Authors:

P. Christiansen, D. Antończyk, J. Baechler, R. Bramm, R. Campagnolo,
U. Frankenfeld, C. Gonzalez Gutierrez, M. Kowalski, B. Mota,
L. Musa, S. Popescu, K. Schossmaier, C. Soos

for the ALICE TPC Collaboration

Abstract:

An Inner Readout Chamber (IROC) of the ALICE TPC, with the final FEE readout and DAQ chain, was tested in combination with the prototype field cage at the CERN PS T10 beam line. The chamber response was studied in detail for the gas mixture, Ne-CO_2-N_2(85.7-9.5-4.8). A gain increase of 40% across the chamber was observed that is likely related to wire-pad geometry variations of the order 80 microns. Cosmic tests showed that this is not a problem with the chambers from the series production.
The spatial resolution was the same as for the standard gas mixture, Ne-CO_2(90-10).
The energy resolution was found to be 9-10% in accordance with the TDR, and the measured mean energy-loss distribution in the relativistic rise region was similar to the ALEPH data for Ar-CH_4(90-10) used in the AliRoot simulations.

Contents

1 Introduction **2**

2 TPC Setup at the T10 Facility **3**
2.1 Data Taking 4

3 Analysis **6**
3.1 Signal 7
3.2 Electrostatic Field Distortions. 10
3.3 Space Point Resolution. 10
3.4 Signal Attenuation due to O_2 12
3.5 Stability 12

4 Energy-loss measurements **13**
4.1 Gain variations 13
4.2 dE/dx curve for the Ne-CO_2-N_2mixture. 18
4.3 Conclusions 22

A PHOS test beam results on beam content. **22**

B Plots from dE/dx analysis. **23**

1 Introduction

Within the TPC project a test facility was build at CERN to study in detail the performance of an IROC in combination with the final electronics and the DAQ readout chain. Tests have been carried out with cosmic triggers and radioactive sources over the last years [1]. By triggering on cosmic ray showers it has been possible to test the performance of the FEE under very high channel occupancies ($\geq 50\%$).
To study the response of the chamber with mono-energetic beam particles, the TPC test setup was installed in the T10 beam line. This allowed to evaluate the gain homogeneity and energy-loss resolution with a high precision. A new gas mixture, Ne-CO_2-N_2(85.7-9.5-4.8), has been proposed to limit the gas gain sensitivity to variations of N_2, due to leaks, and reduce the risk of discharges [1] [2]. By varying the extraction momentum the mean specific energy-loss for a track in the new gas has been measured.
All channels of the IROC were instrumented with the FEE and readout via the ALICE DDL data transfer system (D-RORC and SIU). It should be pointed out that it was the first time that all components were available in a final version. A technical description and documentation of the different subsystems can be found elsewhere [3, 4, 5, 6, 7, 8].

[1]The new gas mixture has the same drift velocity and diffusion coefficients as the standard gas mixture, Ne-CO_2(90-10), but requires a higher sense voltage to achieve the same gain.

In this note the focus is put on the physics performance of the system. General information on the TPC design, chamber production, and earlier tests can be found in [9, 10, 11].

2 TPC Setup at the T10 Facility

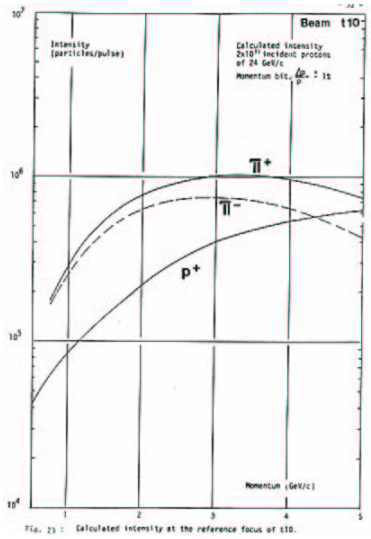

Figure 1: Calculated intensity for $\pi^{\pm}$ and p at the reference focus of T10.

The TPC sector beam test was carried out at the T10 beam line in the PS east hall from May 10th to June 2nd 2004.
The beam at T10 is a secondary beam from the PS accelerator. The momentum of the extracted beam can be adjusted between 1 and 7 GeV/c, positive and negative polarity. The beam profile at the TPC was roughly Gaussian with vertical and horizontal widths between 1.5 and 3.0 cm depending on the settings.
Figure 1 shows the abundances of pions and protons in T10 as a function of beam momentum. The electron and positron admixture of the beam depends on the selected production target. There was no possibility to trigger selectively on these particles. High energy muons (with momentum up to 20 GeV/c) from upstream pion decays which are on beam axis, generated a large background.
The PS east hall beam lines are described in [12] which can be required at the CERN library and is similar to the web documentation [13].
A schematic view of the setup is shown in Fig. 2. For triggering and TOF information we had a setup of four large scintillators (two in front (TOF F) and two in back (TOF B), all horizontal). The active area of the counters was 20×20 cm^2, and the standard trigger required the coincidence of all four counters. The distance between the counters of 14 m and the TOF-resolution of $\sigma_{TOF} \sim 285$ ps allowed a 4σ separation of protons and pions up to $p = 4$ GeV/c.

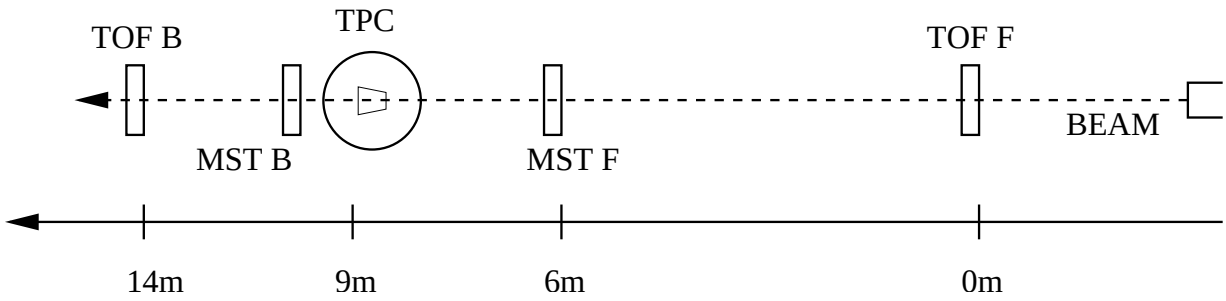

Figure 2: Schematic view of the setup in T10. In front (F) and behind (B) the TPC, scintillators were placed for triggering and measuring the Time-Of-Flight (TOF) and a silicon strip telescope (MST) for tracking the beam.

Finally a Micro Strip Telescope (MST) [15, 16], was used for external tracking. This was included in the data in a few runs with a narrower trigger (FINGER trigger). This trigger setup consisted of four finger scintillator counters, each 1cm wide. One pair of counters were setup as a cross right before the MST F and the other pair right after the MST B. The trigger required coincidence between the signals in all four counters. The MST data have not been used in this analysis where the focus is on the energy resolution.
The test TPC at CERN consists of a prototype field cage in an aluminum cylinder, ~ 2.8 m long with a radius of ~ 70 cm. The central membrane divides the active drift volume in two halves with a maximum drift length of ~ 140 cm. At one end plate, an IROC module has been installed.
The IROC was fully instrumented with $18+25 = 43$ FEC's which corresponds to $43 \times 128 = 5504$ channels or 1 % of the total number of channels in the final TPC. One card was disconnected because of ground problems. The FEC's were controlled by two RCU's (1 for the front 18 cards, and 1 for the back 25 cards).
A specific online monitor was developed for visual inspection of the TPC performance [18]. The online monitoring of the TOF and MST was done using the software tool MOOD [19]. The online monitoring allowed an immediately evaluation of the performance used to adjust the operational parameters.

2.1 Data Taking

A schematic view of the whole DAQ system is shown in Fig. 3. The DATE system version 4.8 [20] was deployed on 4 computers running CERN Red Hat Linux 7.3 as operating system. Three of these computers were used as LDCs to perform the readout, and one computer was used as GDC for the event building. All of them were connected to a Fast Ethernet switch with a 10 MB/s uplink to the CERN backbone.
LDC1 (dual Xeon farm PC) was in charge to handle data streams over the two DDLs to bridge about 30 meters. One DDL channel consists of an SIU, which is attached to an RCU on the IROC, and a dual-channel D-RORC. The latter was configured in splitting mode, hence a copy of all the incoming data stream was put onto a DDL channel going out

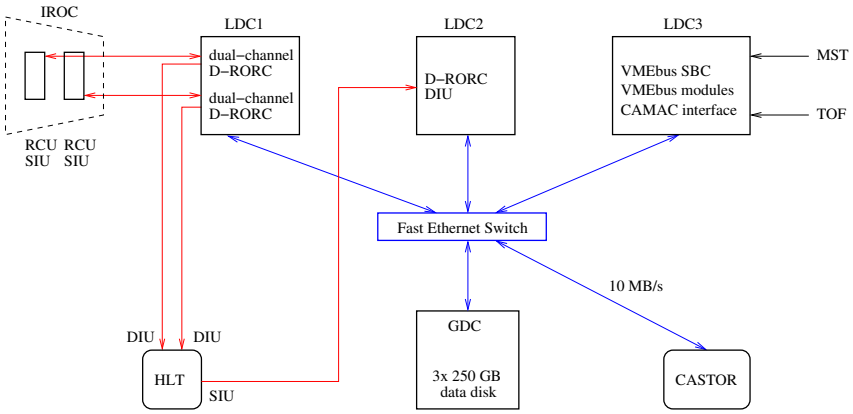

Figure 3: Schematic view of the DAQ setup.

to the HLT system [8]. A further DDL channel funneled the output of the HLT system to LDC2 (dual Xeon farm PC), which was equipped with a single-channel D-RORC. LDC3 (Pentium III PC in VMEbus form factor) performed the readout of the MST and TOF by operating VMEbus modules and a CAMAC interface. In order to keep all date sources (RCUs, VME modules) synchronized, a trigger signal is required for each data source and an external common BUSY signal. This was achieved by setting up a NIM trigger logic similar to the one developed for the SDD test [16]. Finally the GDC (dual Xeon farm PC) assembled the sub-events from the LDCs to a full event, which was based on a simple event counting mechanism. Full events could be recorded to local storage (three 250 MB IDE disks) or uploaded to CASTOR [17].

On the TPC side the data were sampled at 10 MHz frequency by the FEC being twice as high as the nominal 5 MHz ([9] p. 154). The ALTRO action on the FEC allows pedestals to be subtracted online and zero suppression of the data output. These features (and the more sophisticated baseline corrections and tail cancellation filters) were not used during the test, instead black events were recorded. These events include all the samples of all channels. A single channel with 512 time bins is therefore 640 B, and an event with all FEC's is: $42 \cdot 128 \cdot 640$ B $= 3.4$ MB. Since most of the FEC's were outside the area covered by the beam, the number of FEC read out was reduced to $8 + 9 = 17$ and the event size to 1.4 MB. The size of the events from the MST was up to 7 KB, and the TOF produced 16 B events.

Both RCUs were configured via the backward channel of the DDL by using the FeC2 tool which is part of the DATE software kit. As many as 6400 data blocks (of the size 1 KB or 2 KB) and 9600 commands were needed to configure an RCU with 25 FECs. The download itself took less than 1 second.

The total amount of raw data collected in CASTOR was 533 GB covering about 4500 files. A typical run for data taking purpose lasted in the order of 20 minutes (stopped by the operator) with $\sim$ 6000 events. The longest run executed was 1.5 hours with $\sim$ 17000 events. The raw files containing all the pads were first reduced by removing the pads which did not contain an ADC value of at least 6 ADC channels above the baseline after time bin

100 (after the induced gating grid signal). This typically reduced the file size by a factor 10, allowing the files to be written as ROOT-formatted files on a local disk and analyzed from there.

3 Analysis

The analysis was done using the standalone software developed for the cosmic ray tests [1]. In addition the online monitor software to read the raw DATE file format and calculate the baseline was added [18].
The analysis algorithm can be divided in three steps.

Pedestal subtraction

The baseline was evaluated event by event. For each pad the baseline value is calculated in two iterations. In the first iteration the mean of all ADC channels in the time bin interval between 20 and 500 is calculated. In the second iteration the mean is recalculated ignoring ADC channels 10 or more channels away from the first mean. This value in then used for pedestal subtraction.

Clustering

The algorithm used was the same as for the cosmic ray analysis. ADC values which after the pedestal subtraction are 3 or more are filled in a pad-time matrix for each row (this cut is the same as for the final electronics, see Table 7.3 in [9]). Each pad-time cell is then compared to the 4 surrounding cells to mark peaks that are used as seeds for clusters. The clustering is done by searching for signals around the peaks. For a cluster to be accepted it is required to cover 2 or more pads and time bins, and the peak-value (also called the maximum charge Q_{MAX}) must be at least 8 ADC CH.
The cluster is made up from cells and the total charge Q_{T} refers to the sum of the charge in each cell, while Q_{MAX} is the largest value among the cells.

Event selection

Because of the simple structure of the events with tracks covering the full chamber, single track events were selected by a fiducial cut in time coordinate and requiring that the number of clusters was similar to the number of rows. For clusters with large charge deposits it was found that the clustering algorithm sometimes produced double clusters (1 out of 100). The effects of this has been carefully studied and found to have no effect on the results presented here.

Summary of cuts applied to the data

The analysis contains the following cuts after pedestal subtraction and ignoring the early channels :

- Pad signal of at least 6 ADC CH (reduction).
- Cells with signal less than 3 ADC CH are removed (clustering).
- The maximum cluster charge has to be at least 8 ADC CH (clustering).
- The cluster has to have at least 2 pads and time bins (clustering).
- The time coordinate must be within a 100 time bins window (event selection).
- The number of clusters, N_C, must be $60 \leq N_C \leq 64$ (event selection).

The Altro action of the FEC can be simulated by a software algorithm [1, 18]. This was not done for the results shown here. A similar analysis has been done with the Altro action applied without observing any significant differences.

3.1 Signal

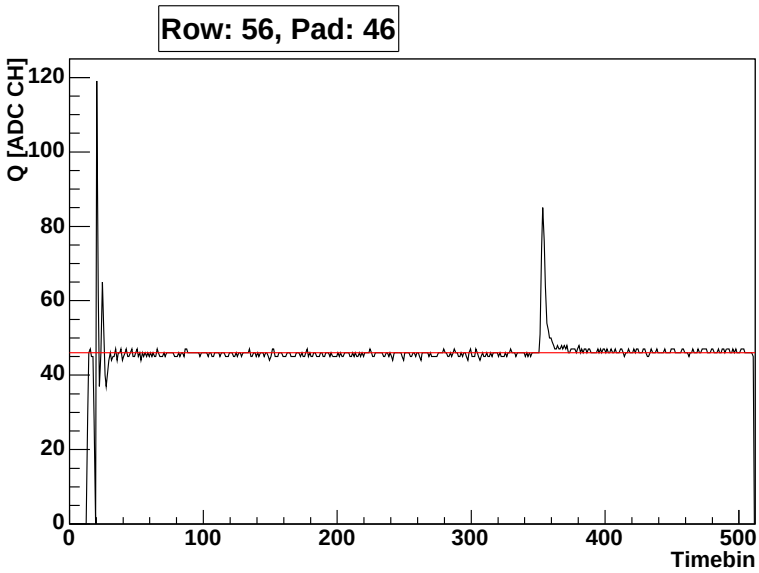

Figure 4: A typical signal on a pad. One time bin corresponds to 100 ns.

Figure 4 show a typical signal on a pad. The first 14 time bins were used by the RCU for pre sampling, then the induced signal follows, showing the opening of the gating grid. Around time bin 350 the signal produced by the charged track is seen.

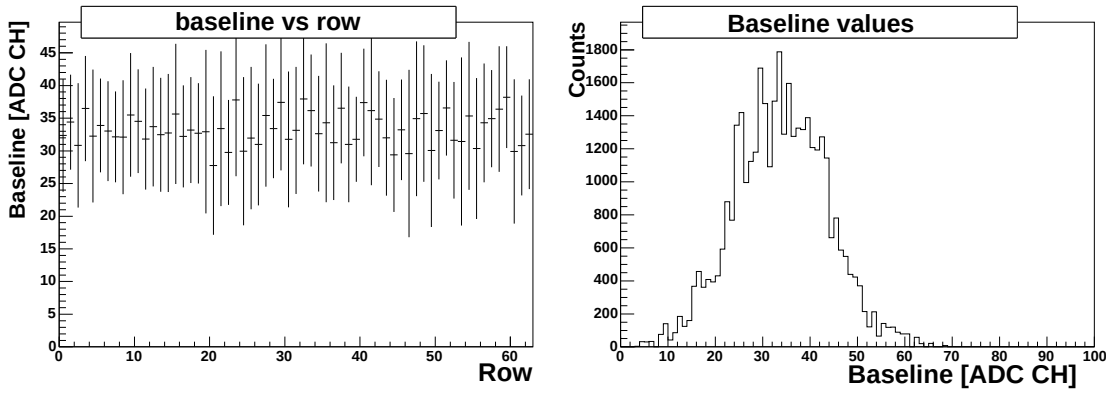

Figure 5: Baseline and gate-peak studies for run 769 ($\sim$ 150 events). Left: Baseline vs row (error shown is RMS). Right: Distribution of baseline values.

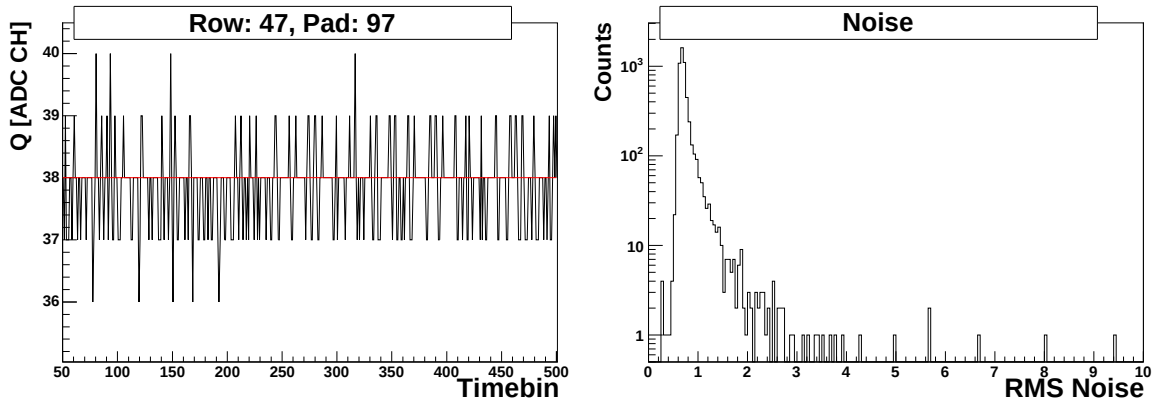

Figure 6: Left: Plot of the pedestal signal for a single pad. Right: The distribution of RMS noise for all pads.

The average baseline for each row and the distribution of baseline values are shown in Figure 5.
The noise, σ_{NOISE}, for each pad can be calculated in pedestal runs as:

$$\mu = \frac{\sum_{i=50}^{i=499} \mathrm{ADC}_i}{450} \quad (1)$$

$$\sigma^2_{\mathrm{NOISE}} = \frac{\sum_{i=50}^{i=499} \mathrm{ADC}_i \times \mathrm{ADC}_i}{450} - \mu^2 \quad (2)$$

$$(3)$$

The obtained noise level for each pad is shown in Figure 6. The requirement in the TDR is to have $\sigma_{\mathrm{NOISE}} \leq 1$ ADC (~ 1000 electrons), and this is achieved for 93% of the channels (without any pre selection on the Altro chips).

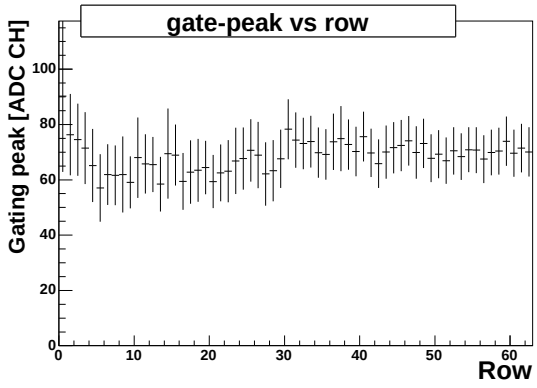

Figure 7: Gate-peak value vs row (error shown is RMS). The first RCU covers the first 30 rows, while the second half is covered by the second RCU.

Figure 7 shows the distribution of the gating peak signal height as a function of row. The induced signal for the first 30 rows (read out by RCU1) is slightly lower than for the last rows (RCU2). This might be caused by the specific distribution of the gating signal.
For the new gas mixture the optimal working point had to be determined. Figure 8 (left panel) shows the most likely value of Q_{MAX} scaled to the MIP value (not the average since it is approximately Landau distributed) as a function of sense voltage applied. The chosen value of 1480V was found by looking at the monitor signals. The signal to noise for the IROC of 1:20 ([9] p. 147) is fulfilled for this chosen sense voltage. For a MIP cluster, the typical number of pads covered is 2-4, number of time bins is 6-9, and the total number of cells 15-20. For the nominal sampling frequency of 5 MHz, the number of time bins and cells is approximately halved. This implies that for the nominal setup most clusters will cover 3 or more pads and time bins leading to a good determination of the charge centroids (space position) in both directions.
The final parameters for the system is shown in Table 1.

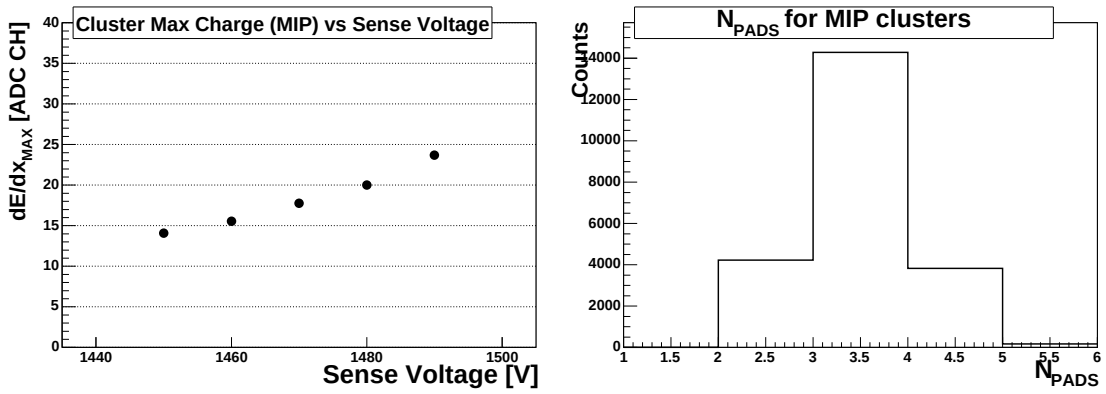

Figure 8: Left: This is the most likely value of the maximum charge as a function of HV scaled to the MIP value for the HV runs. Right: The number of pads per cluster for a MIP (3 GeV/c proton) with the chosen sense voltage of 1480 V.

Sense Voltage	1480 V
Gate Voltage	130 ± 100 V
Drift field	400 V/cm (nominal)

Table 1: The final voltage settings determined in the test beam.

3.2 Electrostatic Field Distortions.

If the drift field is not homogeneous, track distortions can be introduced. These distortions can be described as systematic deviation from straight line tracks. In Figure 9 the average pad and time coordinate for clusters are shown as a function of row position. The origin of track distortions is due to the imperfect adaption of the readout chamber to the drift field. Therefore the distortions are largest close to the edges.

3.3 Space Point Resolution.

If the straight line fit is restricted to the rows in the middle of the IROC, then the distortions are small and the resolution can be estimated from the residuals. Figure 10 shows the obtained distribution of residuals in the pad and time direction for a straight line fit to the clusters in row 21-40. The width of the distributions, δ_{PAD} and δ_{TIME}, are expected to be:

$$\begin{aligned} \delta^2_{\mathrm{PAD}} &\sim \delta^2_{\mathrm{PAD},0} + \frac{D_T^2 \cdot s_{drift}}{N_{e^-}} \\ \delta^2_{TIME} &\sim \delta^2_{TIME,0} + \frac{D_L^2 \cdot s_{drift}}{N_{e^-}}, \end{aligned}$$

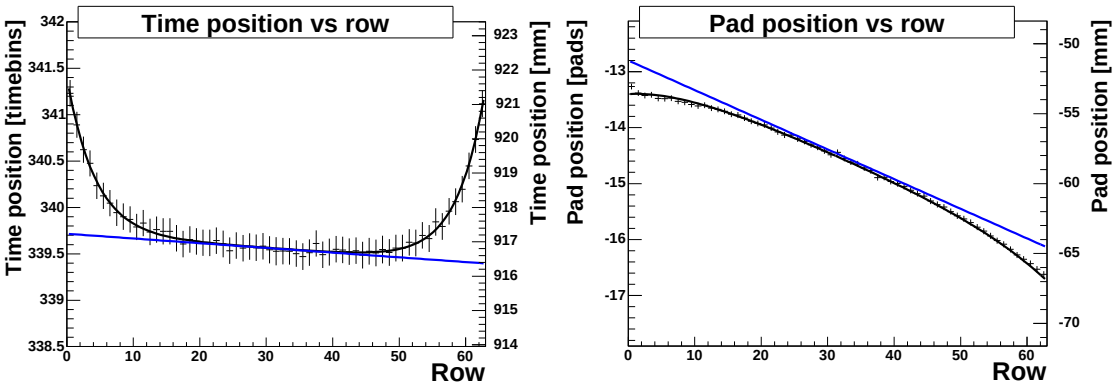

Figure 9: The distortions of the track in the prototype TPC field cage. The black curve is a fit/parametrization (left/right) with a linear term and two exponential terms.

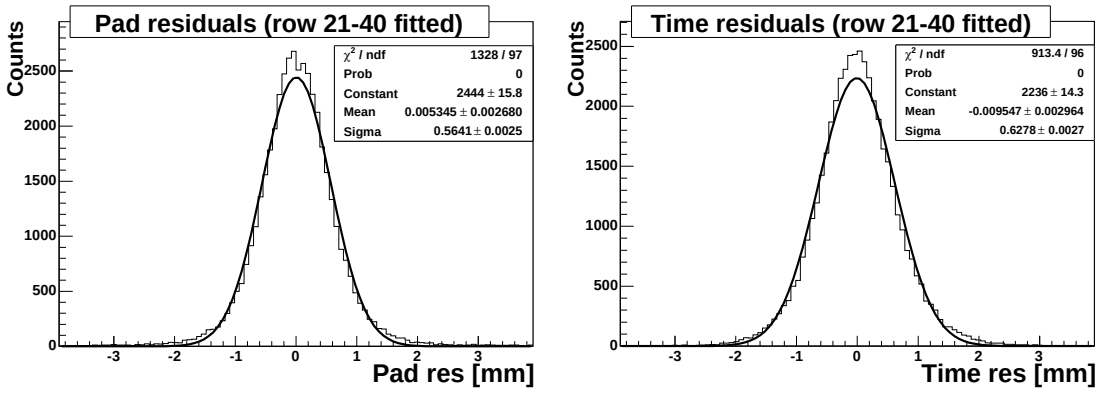

Figure 10: The pad and time residuals (assuming $v_{drift} = 2.8$ mm/μs) for a straight line fit to the clusters in row 21-40.

where $\delta^2_{\mathrm{PAD},0}$ and $\delta^2_{TIME,0}$ is the intrinsic resolution, D_T and D_L is the transverse and longitudinal diffusion coefficients respectively, $D_T = D_L = 220\mu\mathrm{m}/\sqrt{\mathrm{cm}}$ [9, 2], $s_{drift} = 1$ m is the drift length, N_{e^-} is the total number of ionized electrons per row length, $N_{e^-} \sim 30$ [9]. Then we find that the contribution from diffusion is in both cases $\delta_{DIFFUSION} \sim 400\mu$m. The fluctuations of the gas gain contributes with an additional factor $\sqrt{2}$ [9], so the final final contribution from diffusion is of the same order as the measured resolution indicating that the intrinsic resolution is significantly smaller.

3.4 Signal Attenuation due to O_2

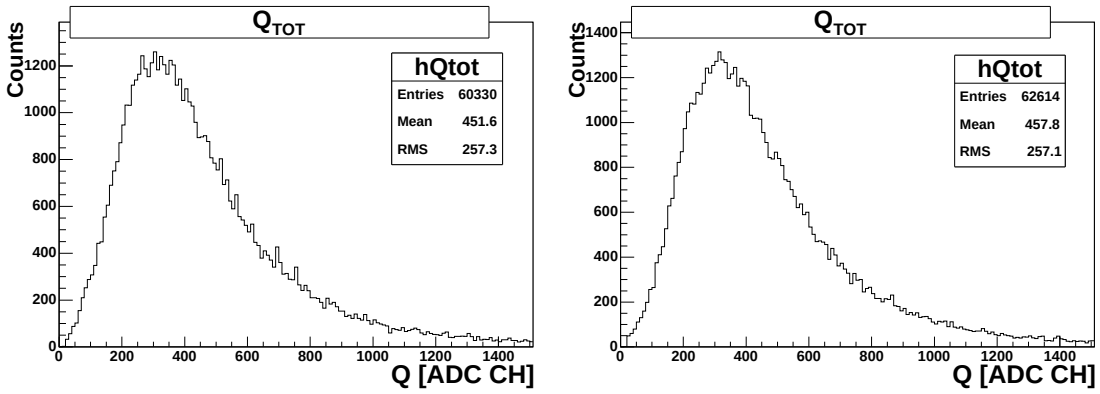

Figure 11: Left: The charge distribution for the normal setup with a drift length of ~ 1 m. Right: The same distribution, but with a 28 cm shorter drift length.

A set of two runs was devoted specifically to estimate the O_2 content in the drift gas. The effect of O_2 molecules in Ne-CO_2 is an electron attachment (charge loss) of 1% per ppm per m oxygen, $N(O_2)$ [9].
First a run with nominal settings was recorded and then the TPC was shifted, resulting in a 28 cm shorter drift distance, and a second run was recorded. The total charge distributions measured in the two runs are shown in Figure 11.
The final number of electrons before amplification, $N_{e^-,\mathrm{FINAL}}$ to the initially ionized, $N_{e^-,\mathrm{INITIAL}}$:

$$N_{e^-,\mathrm{FINAL}} = N_{e^-,\mathrm{INITIAL}} \cdot e^{-k \cdot N(O_2) \cdot s_{\mathrm{drift}}} \tag{4}$$

where $k = 0.01$ m^{-1}.
Fitting the two peaks of the charge distribution and taking the ratio, r, one finds: $r = 322.5/315.5 = 1.022$. From Eq. 4 one then finds $N(O_2) = \log(r)/(k \cdot \Delta s_{\mathrm{DRIFT}}) = 8$ ppm.

3.5 Stability

The longest run was approximately 30 minutes and in this time the average dE/dx is stable, see Figure 12. The variation of the external parameters (temperature and pressure) during the time of a single run are small and do not alter the dE/dx stability.

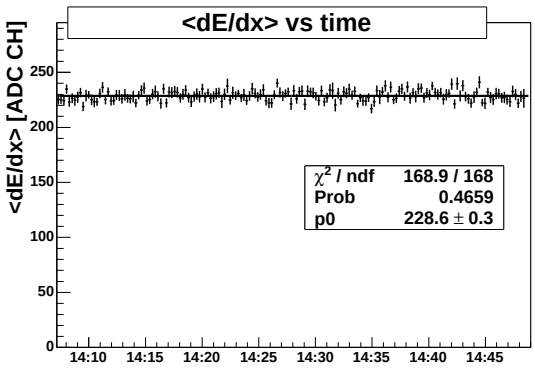

Figure 12: The average dE/dx as a function of time in a single run.

4 Energy-loss measurements

For the energy-loss measurements both the total charge Q_{T} and the maximum Q_{MAX} is used. To obtain the energy-loss for a track a truncated mean is used where the 10 % lowest values and the 30 % highest values are discarded. Different cuts for the truncation was compared (10-70 (used here), 0-60, 0-70) and found to give the same energy resolution. The truncated mean is here denoted dE/dx when done for Q_{T} (and has the subscript MAX when done for Q_{MAX}).

4.1 Gain variations

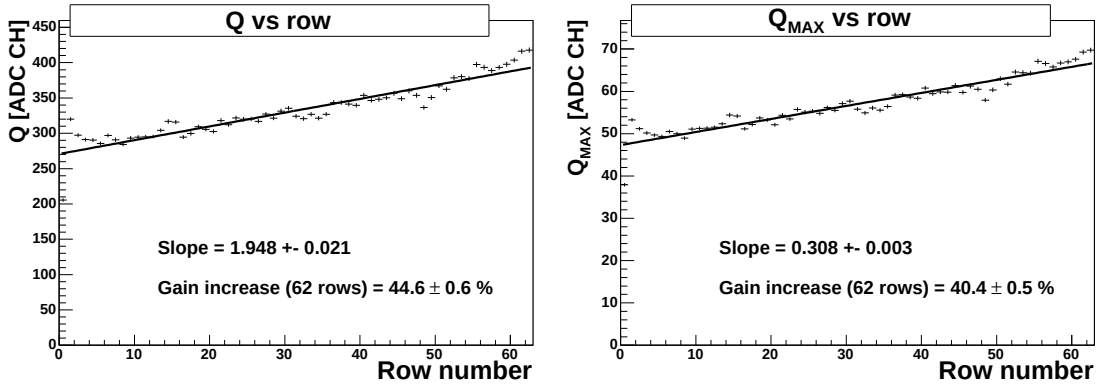

Figure 13: The average cluster charge (left) and cluster maximum charge (right) as a function of row number.

The average cluster charge in a row, $\langle Q \rangle_{\mathrm{ROW}}$, can be defined as:

$$\langle Q \rangle_{\mathrm{ROW}} = \frac{\sum Q_{\mathrm{ROW}}}{N_{\mathrm{TRACKS}}} \tag{5}$$

where N_{TRACKS} is the number of events with single tracks.
During the detailed analysis of the data, a gain variation with the row number was observed. The average cluster charge and cluster maximum charge shown in Figure 13 varies as a function of row. The low row numbers are those with shortest sense wires. The gain variation as a function of pad row is fitted with a linear fit: $\langle Q \rangle_{\mathrm{ROW}} = \alpha \cdot \mathrm{row} + \beta$.
Assuming that the average charge and the gain, $G(\mathrm{row})$, is related as $\langle Q \rangle_{\mathrm{ROW}} = k \cdot G(\mathrm{row})$, the gain increase is expressed as

$$\frac{G(62) - G(0)}{G(0)} = \frac{(\alpha \cdot 62 + \beta)/k - \beta/k}{\beta/k} = \frac{\alpha \cdot 62}{\beta}. \tag{6}$$

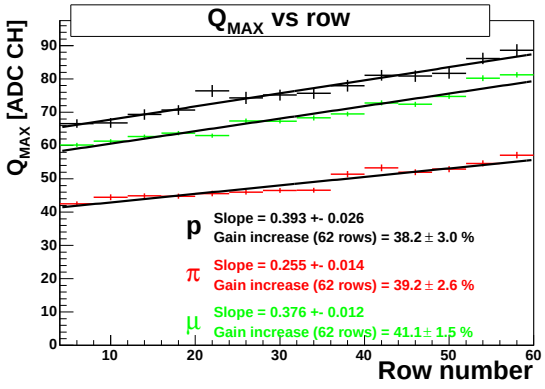

Figure 14: For different particle species in the same run the gain increase is the same within statistical errors while the slope is different.

Figure 14 shows the gain increase for protons, pions and muons in a single run (see Figure 21 for PID). For each particle specie the slope, β is different, while the gain increase is constant. Therefore we will focus on the gain increase in the following.
The gain increase of the total cluster charge is larger than for the maximum charge. This is due due to the clustering algorithm which suppresses the small ADC values, so it is sensitive to more details of a cluster with a large signal.
The cluster shape shows only small differences across the chamber.
For the same configuration of the TPC settings, see Table 1, similar variations were seen in all runs, as shown in Figure 15.
For the cosmic ray data taken in 2003, the standard gas, Ne-CO_2(90-10), was used. This gas requires a lower anode voltage for the same gain (1250 V vs 1480 V). Due to this lower anode voltage the observed gain increase lower ($\sim 20\%$), see Figure 16.
Since the induced gating signal and the pedestals do not show a similar behavior, see Figure 5 and Figure 7, the gain increase is most likely a property of the chamber.

Measurements done at GSI with IROC #1

The chamber was taken out and send to GSI for further studies [21]. It was found that there was no problem with the wire tension, so that the effect is not related to anode wire

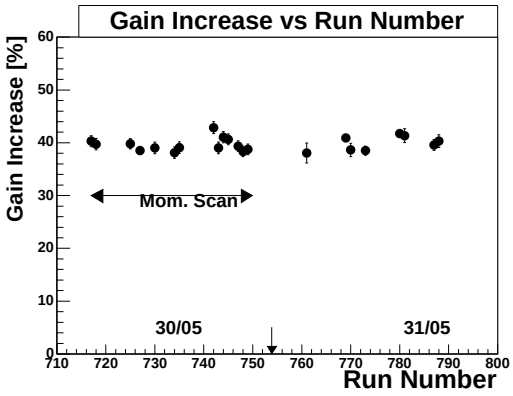

Figure 15: The gain increase of Q_{MAX} from row 0 to row 62 for different runs, including a momentum scan, over a two day period.

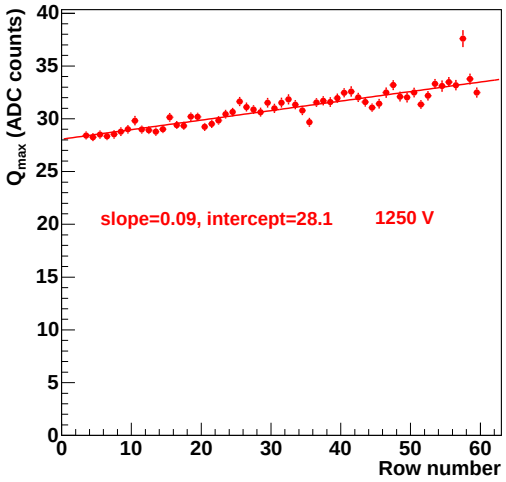

Figure 16: Q_{MAX} as a function of row number in the cosmic data runs. The gain increase is also observed there.

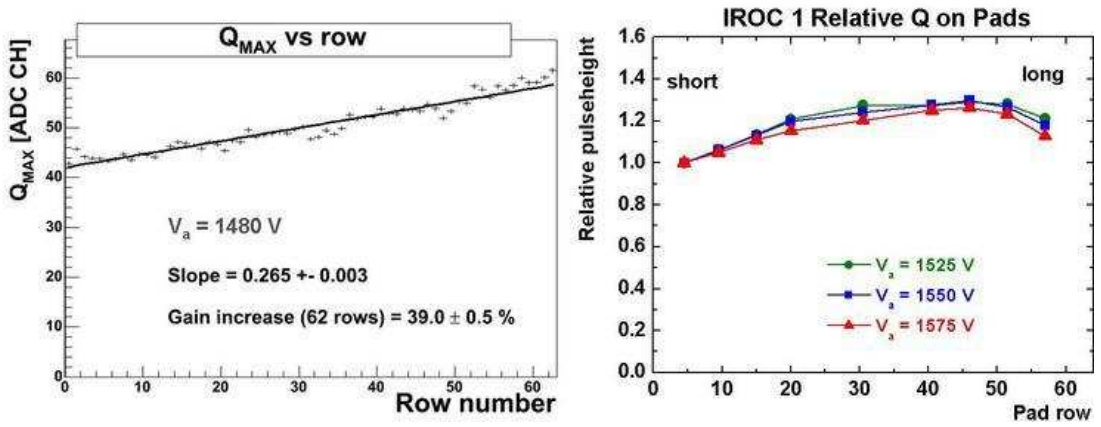

Figure 17: Comparison of test beam data (left) and source measurement at GSI (right). The vertical scales have been aligned. The qualitative same behavior is observed, but while the test beam data increases almost linearly with row number the source scan data flattens out and decreases from row 30 and onward.

sagging. A setup for making measurements with a radioactive Fe-55 source exists at GSI. The collimated source is positioned over the pad-row plane and the integrated current on the pads is measured. By shifting the position of the source it is possible to scan the chamber. A precise source scan was carried out and the results showed good qualitative agreement with the test beam measurement, see Figure 17, but the gain increase is smaller for the long anode wires.

Geometrical survey of IROC #1 at CERN

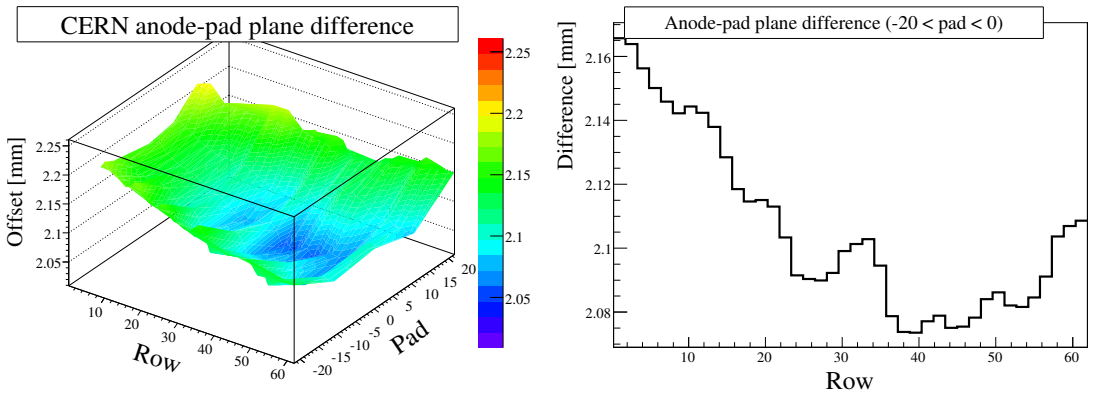

Figure 18: The measurements of the distance between the anode wire plane and the pad plane at the metrology workshop. Full chamber (left) and projection in the test beam acceptance (right).

Calculations using Garfield and Magboltz shows that gain variation fluctuations of the

same magnitude as observed can be caused by imperfect geometry of the anode wire plane with respect to the pad plane [21].
The IROC #1 was send back to CERN and surveyed at the metrology workshop at CERN. The chamber was positioned on the three alignment pieces and the anode wire plane and pad plane was surveyed at 190 positions with a resolution of 3 microns. The resulting anode-pad plane difference is shown in Figure 18 together with the projection along the pads where the TPC test beam measurements were done. The survey shows that the distance decreases almost linearly for the first 40 rows (gain increasing) and then increase slightly for the last 23 rows (gain decreasing).

Comparison of measurements with IROC #1

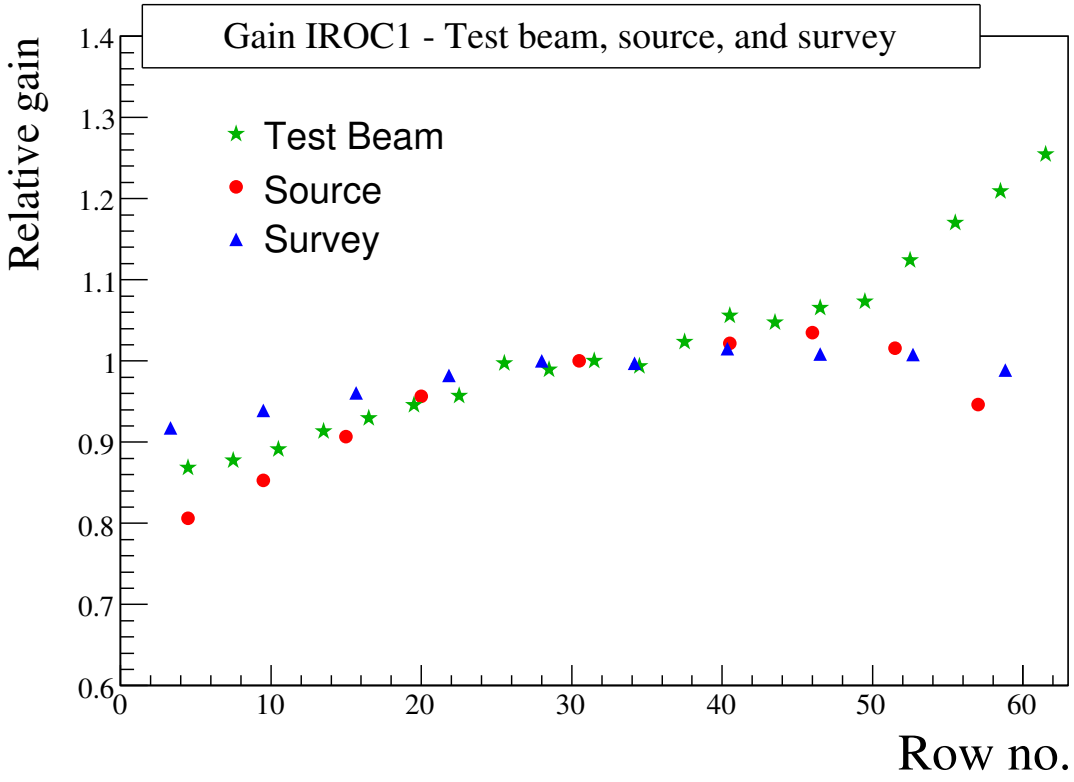

Figure 19: Comparison of the relative gain vs row measured in the test beam, with the source, and estimated from the survey data. All measurements have been normalized to 1.0 around row 30.

Using the calculations of the gain dependence on the anode-pad distance [21], it is possible to relate the survey data with a gain variation. Figure 19 shows the comparison of the test beam, source, and survey measurements of IROC #1. The survey data shows the smallest fluctuations of the gain, but the calculations do not take into account the coupling to the pads which would increase the variations. There are quantitative differences between the

three measurements, but given the fact that the three measurements are very different they show a remarkable similar qualitative picture which suggests that the observed gain variation in IROC #1 can be explained by the mechanical tolerances.

Cosmic Ray Measurements with IROC #5

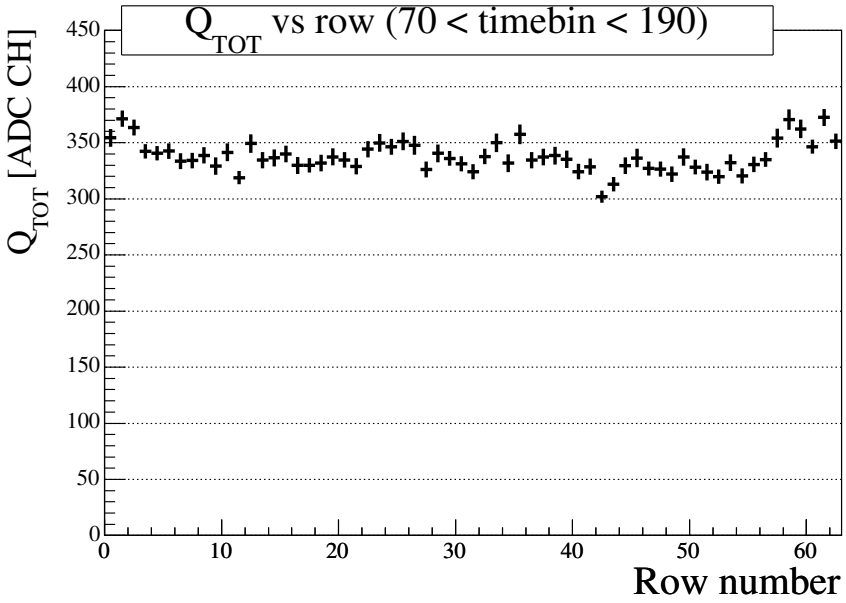

Figure 20: The average cluster charge as a function of row number for IROC #5. The RMS is 4% of the mean.

A new IROC was installed in the test TPC and cosmic ray data were collected in April 2005 with the old gas mixture Ne-CO_2(90-10) at an anode voltage of +1440V. The new IROC, IROC #5, represents the quality of the serial production. The results on gain variations are presented in Figure 20. No systematic dependence on the row number is observed.

4.2 dE/dx curve for the Ne-CO_2-N_2mixture.

Figure 21 (top) shows the measured TOF vs the truncated charge dE/dx for the $p = +1$ setting [2]. Three particle species can be identified. The protons and pions were easily identified by TOF and energy-loss while the last species was identified (using PHOS test beam results) as background muons with momentum $p \sim 15$ GeV/c, see A.
The TOF allows the protons to be separated from pions and muons for momenta $p \leq 4$ GeV/c. The energy resolution, σ_E, and the energy-loss, E, can then be obtained by

[2]The + and − used with momentum here indicates if negatively or positively charged particles were selected.

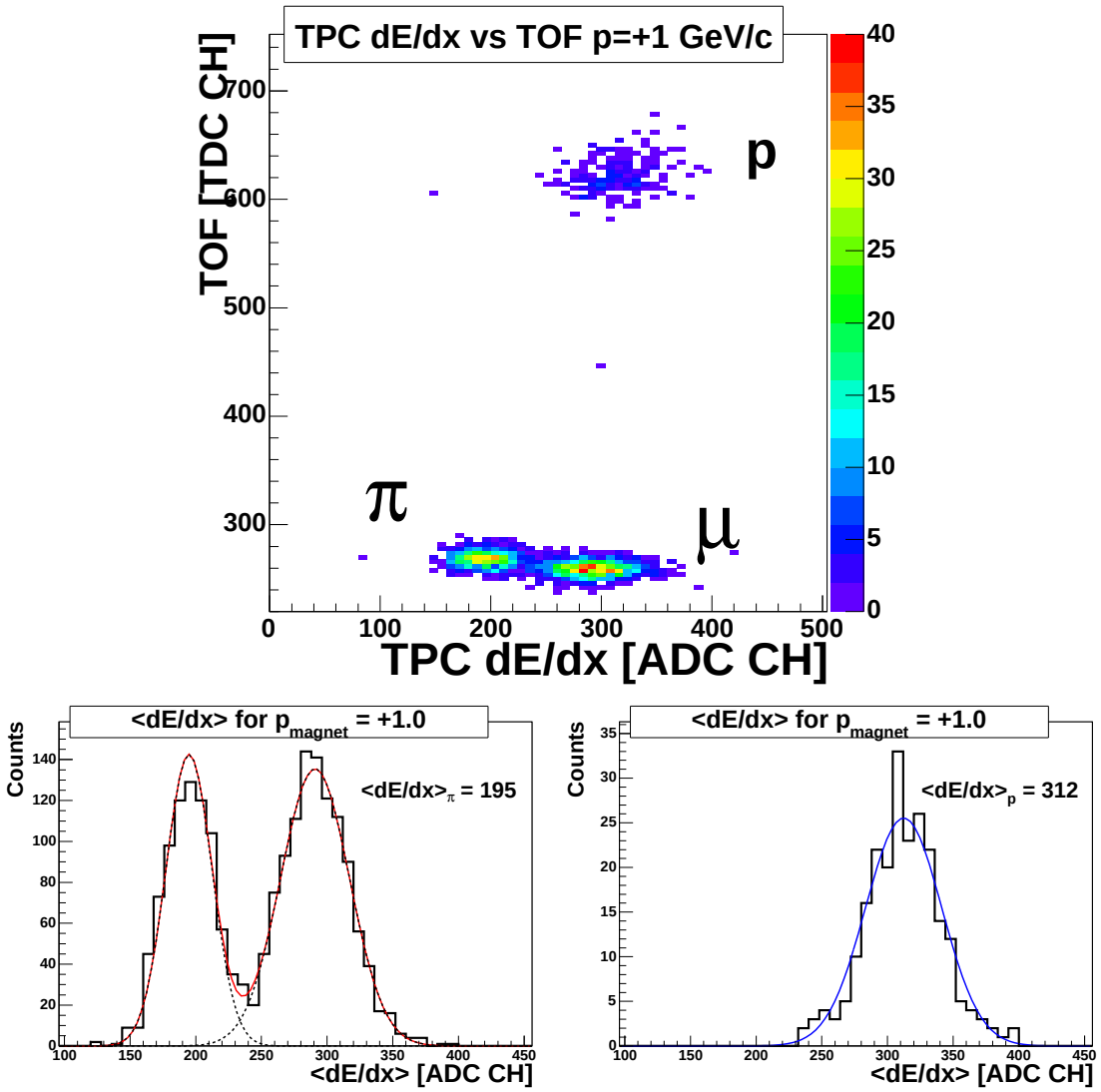

Figure 21: dE/dx distribution for pions and background muons (left), and protons (right) for momentum $p = +1$ GeV/c.

fitting the dE/dx distributions with a single Gaussian for the protons and a sum of two Gaussians for pions and muons, see Figure 21 (bottom).

Momentum	σ_E (π/μ)	σ_E (p)
+1	9.0 %	8.3 %
+2	9.5 %	9.9 %
+3	9.2 %	9.4 %
+4	9.3 %	9.7 %

Table 2: The energy-loss resolution obtained from likelihood fits (slightly larger than for χ^2 fits) for different momentum settings.

The systematic study of the energy resolution is summarized in Table 2. The energy resolution is slightly better for larger charge deposits which can be seen from the $p = +1$ proton resolution.
The relative energy resolution, σ_E, is found to be $\sigma_E \sim$ 9-10%. If this is scaled from the 63 rows in the test, to the full 160 rows (where the track length is 3 times longer), one finds: $\sigma_E(ALICE) \sim \sigma_E(IROC)/\sqrt{3} \sim$ 5-6 %, 5 % was estimated in the TDR. It is important to note here that the dE/dx energy resolution depends on the total track length and not the number of samples for pad lengths of 1 cm and longer, see Figure 4.16 in [9].
For the energy-loss curve a fixed energy resolution of 9 % was used for the spectra with pions and muons.
To study the effects on the energy-loss measurement caused by the gain variations (section 4.1) the same analysis was done for three subsets of the rows, low (row 2-21), medium(22-41), high(42-61). The results are shown in Figure 22. The relative resolution is the same for the three subsamples and the resolution using all 60 rows is approximately a factor $\sqrt{3}$ better, so no effect is observed, but in this test we have full tracks with hits in all rows. For a full simulation of the ALICE TPC with similar variations in inner and outer sector, it was verified that even without calibrations the resolution is changed by less than 10% (from 6.2% to 6.6 % for full lengths tracks) [22].

A set of 14 runs recorded within $\sim$ 7 hours, with beam momentum $-1, -2, ..., -7, +1, +2, ..., +7$ has been used for the dE/dx analysis of the new gas mixture. The fit to the dE/dx distributions for the positive settings are shown in appendix B (Figure 26 and Figure 27). The obtained energy-loss curve is shown in Figure 23. The left figure shows the energy-loss in ADC CHs. The statistical error is less than 1% so the small discrepancies between measurements at similar values of $\beta\gamma$ are likely related to changes in temperature and pressure over the time of the measurements, e.g., the ratio between the muon energy-loss and the pion energy-loss is the same for positive and negative polarity setting even though the respective values are different.
Figure 26 (right) shows the data normalized to 1 at the minimum, and compared to two reference curves. The reference curves are the ALEPH Ar-CH_4(90-10) parametrization

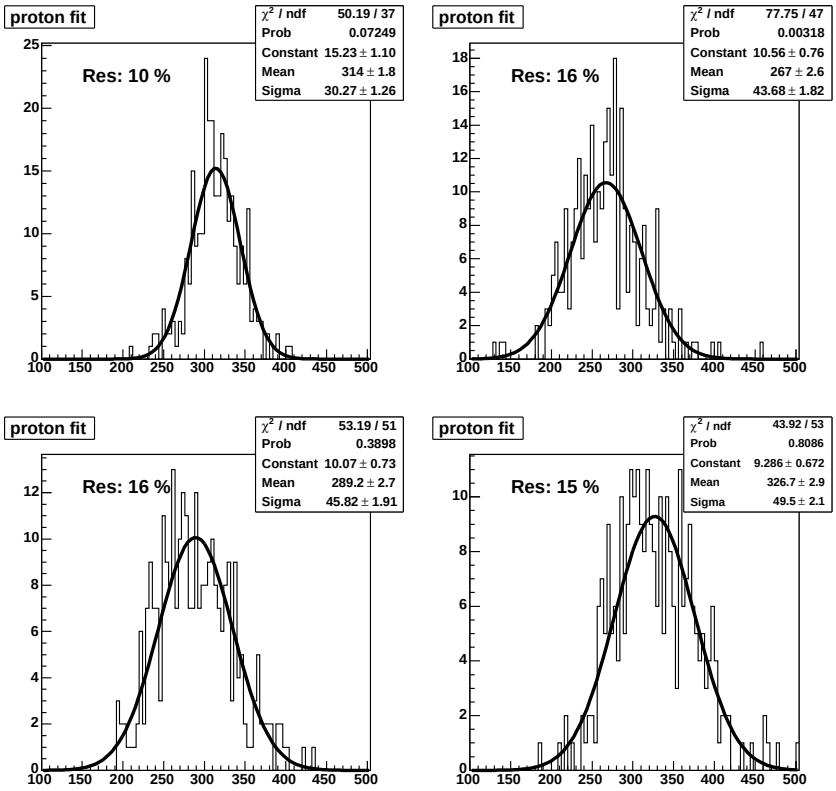

Figure 22: The energy resolution for 1 GeV/c protons. Top left: 60 rows (2-61). Other plots: 20 rows, top right: 2-21, bottom left: 22-41, and bottom right: 42-61.

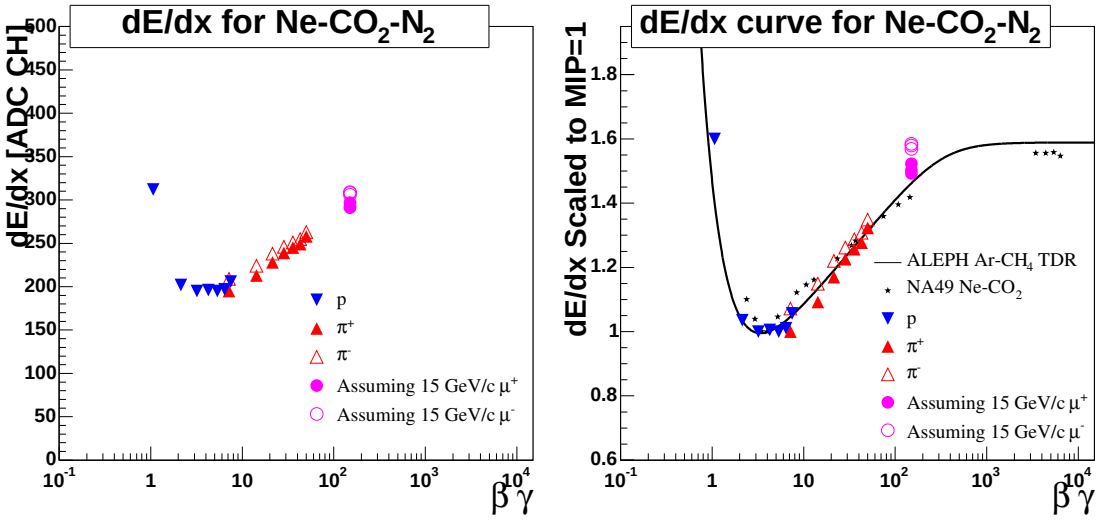

Figure 23: The measured truncated cluster charge as a function of $\beta\gamma$. Left: The measured charge in ADC channels. Right: Scaled to 1.0 for a MIP and compared to the TDR curve and NA49 Ne-CO_2 data [23].

used in the TDR [9], and the NA49 measurements for Ne-CO_2(90-10) [23]. All curves have similar shapes suggesting that the TDR curve used for the simulations is adequate.
When a similar analysis is done for the truncated maximum charge the relative difference becomes smaller, see Figure 25. In the study of gain variations it was observed that the large clusters has an extra gain because the tails are preserved and this might explain the difference between Figure 23 (right panel) and Figure 25.

4.3 Conclusions

The integration of all components worked.
From the results presented in this note we have seen that:

- The spatial resolution of the new gas mixture was found to be similar to the standard gas mixture.
- A gain increase of $\sim 40\%$ as function of pad row number was observed (using the new gas mixture) which can be explained by the mechanical tolerances. For IROC #5 representing the quality of the serial production these gain variations were not observed.
- The energy-loss resolution was found to be $9-10$ %, which agrees with the expected value in the TDR.
- The dE/dx curve for the new gas mixture has been measured and found to be similar to the curve used for the simulations so far.

A PHOS test beam results on beam content.

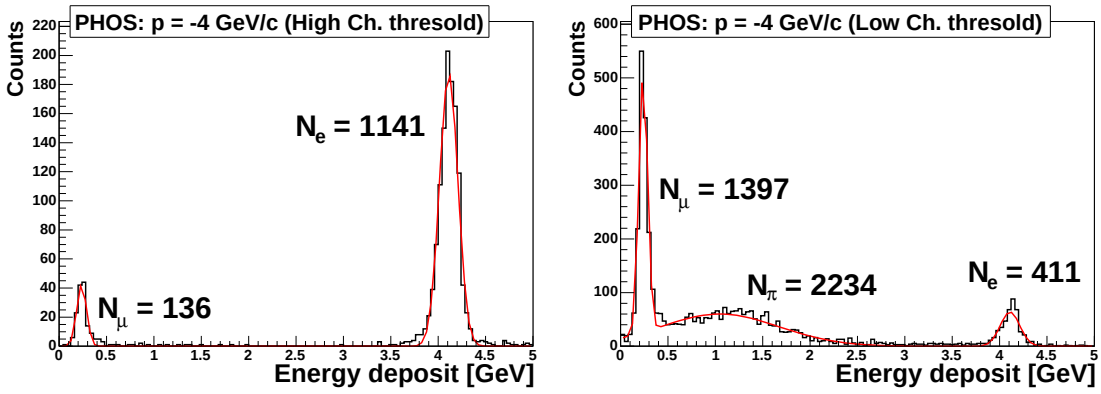

Figure 24: Measurements of the energy-loss of beam particles with the PHOS detector that has triggered the Cherenkov at a high threshold (left) and low threshold (right).

The third species was found to be faster than muons with the same momentum and the energy-loss indicated $\beta\gamma \geq 100$. This indicated that it was either electrons/positrons or background muons (a muon background had been reported earlier at the T7 beam line [24]). The ALICE PHOS group did a scan of the beam line with a Cherenkov trigger. The energy deposit was calculated as sum of energies in 3×3 detectors, when the particle hit the central one. Figure 24 shows the results of the measurement at $p = -4$ GeV/c with two different pressures in the Cherenkov. The length of the PHOS crystals corresponds to 20 radiation lengths and 1 nuclear interaction length. The electrons are identifiable in both plots at maximum energy-loss. The pions can be seen in the right plot as a broad peak around 1 GeV. Muons trigger the Cherenkov, but have negligible energy-loss in the PHOS (same as for the pions that do not interact). From Figure 24 it is estimated that there is 411 electrons, 2234 pions and $1397 - 0.37 \cdot 2234 = 570$ muons. Since no muons from pion decays are observed at $p = 1$ GeV/c, it seems unlikely that these 4 GeV/c muons are from pion decays, i.e., with beam momentum. There are therefore strong indications that this is background muons with momentum $10 \leq p \leq 24$ GeV/c. Here $p = 15$ GeV/c was assumed.

B Plots from dE/dx analysis.

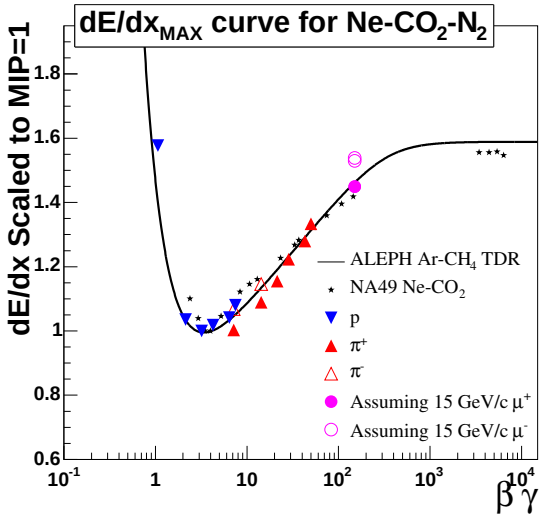

Figure 25: Same as Figure 23, but for the truncated maximum charge instead of truncated charge. Note that the high $\beta\gamma$ points (3%) and the low p point (1.5%) has a lower ratio to the MIP than for the total charge.

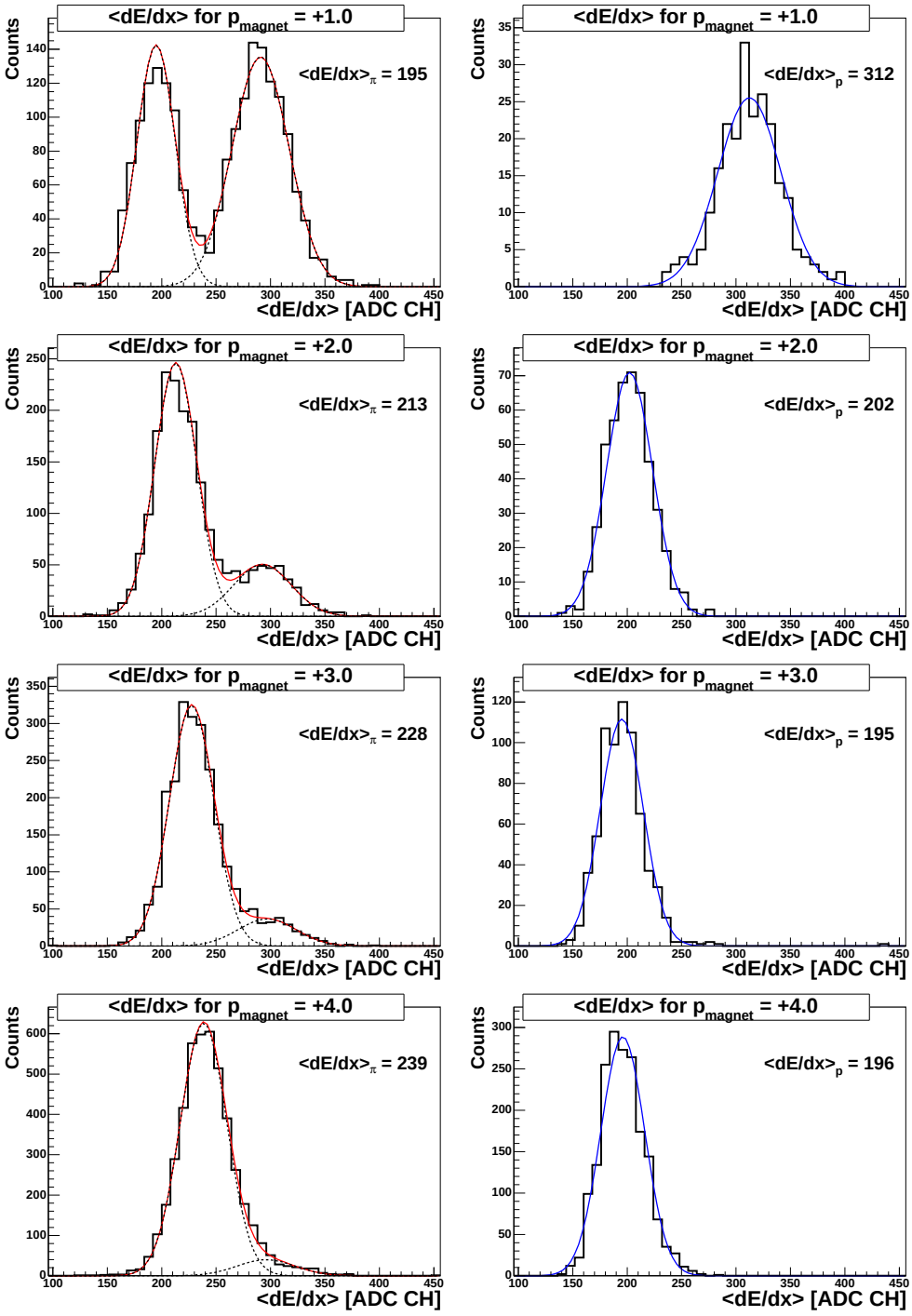

Figure 26: dE/dx distribution for pions and background muons (left), and protons (right) for momenta p =1–4 GeV/c.

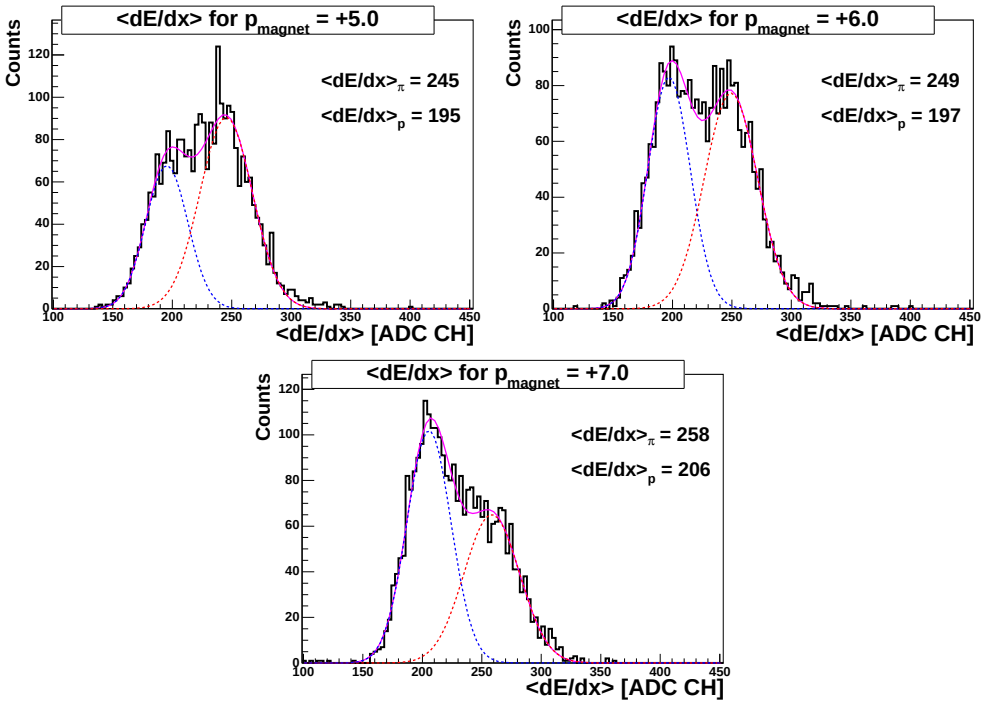

Figure 27: dE/dx distribution for pions (right gauss) and protons (left gauss) for momenta p =5–7 GeV/c.

References

[1] "Cosmic ray measurements with TPC prototype", M.Kowalski, M.Ivanov (ALICE Club 17/11-2003)

[2] "More about Nitrogen", C. Garabatos (TPC meeting in Heidelberg, 12-13/02-2004)

[3] "The TPC Sector Test", P. Christiansen (ALICE week Colmar 23/6-2004)

[4] "Front End Electronics - Preliminary system performance", R. Campagnolo (ALICE TPC meeting Sardinia 16-17/5-2004 - presentations can be found at: `http://www-new.gsi.de/forschung/kp/kp1/experimente/alice/tpc/Sardinia_05_2004.html`)

[5] "Progress on the RCU Prototyping", B. Mota (ALICE TPC meeting Sardinia 16-17/5-2004)

[6] "DAQ system of the TPC sector test", K. Schossmaier (ALICE week Colmar 21/6-2004)

[7] "DCS - Test beam setup", U. Frankenfeld, S. Popescu (ALICE TPC meeting Sardinia 16-17/5-2004)

[8] "HLT - TPC Test Beam", H. Tilsner (ALICE week Colmar 23/6-2004)

[9] "Time Projection Chamber", ALICE TDR, Alice Collaboration

[10] "The ALICE TPC Inner Readout Chamber: Results of Beam and Laser Tests", U. Frankenfeld et al., ALICE-INT-2002-030

[11] "The ALICE TPC Readout Chamber: From Prototypes to Series Production", H. Stelzer et al., ALICE-INT-2003-017

[12] "Secondary Beams for Tests in the PS East Experimental Area", K. Bätzner, D. Dumollard, D.J. Simon, F. Cataneo, M. Ferro–Luzzi, PS/PA/EP/NOTE 88-26 (1988)

[13] http://ps-div.web.cern.ch/ps-div/Reports/PA9321/Welcome.html

[14] http://test-alicetpc.web.cern.ch/test-alicetpc/

[15] http://piotr.home.cern.ch/piotr/TestBeamRef/power_supply.htm, http://test-alicetpc.webtest.cern.ch/test-alicetpc/shiftlist/mstdoc.ps

[16] http://nouais.home.cern.ch/nouais/beamtests/public/bt_2003_08/setup_daq.html

[17] http://castor.web.cern.ch

[18] R. Bramm, Ph.d. thesis, arXiv:physics/0501052

[19] http://cern.ch/alice-daq/MOOD

[20] "ALICE DATE User's guide (DATE V4)", Alice Daq Project, http://cern.ch/alice-daq/

[21] "TPC ROC gain uniformity", C. Garabatos (Technical Board, 13/12-2004)

[22] "dE/dx simulations", M. Kowalski (TPC meeting at CERN, 7-8/1-2005)

[23] "Particle Identification in the NA49 TPCs", B. Lasiuk for NA49, Nucl.Instrum.Meth.A409:402-406, 1998,
"On the Specific Energy Loss in the VTPCs", B. Lasiuk, NA49 note

[24] http://psdoc.web.cern.ch/PSdoc/acc/minutes/2002week27.doc